Analysis of Common- and Differential-Mode HF Current Components in PWM Inverter-Fed AC Motors

Gabriele Grandi, Domenico Casadei, Ugo Reggiani
Dept. of Electrical Engineering - University of Bologna
viale Risorgimento 2, 40136 - Italy

Abstract - In this paper an inverter-fed AC motor drive is analyzed in order to predict the conducted interferences at both the input and output sides of the inverter. HF lumped equivalent circuits for the inverter and the motor stator winding are proposed. The equivalent circuit allows time- and frequency-domain analysis to be performed with standard circuit simulators. The overall circuit model is verified by experimental tests carried out on a prototype of the AC motor drive. The proposed circuit model allows the prediction of the main common- and differential-mode HF current components.

I. INTRODUCTION

The decreasing commutation times of power semiconductor switches made it possible to increase the carrier frequency in PWM inverter-fed motor drives. As a consequence, the motor windings are subjected to a very large amount of HF voltage components [1],[2]. Owing to parasitic winding capacitances [3] (i.e., turn-to-turn and turn-to-iron capacitances), these HF voltage components cause HF leakage currents [4] and conducted Electromagnetic Interferences (EMI) in the power main and the ground system [5],[6]. The resulting HF currents are usually classified in Common- and Differential-Mode (CM and DM) components according to their circulation path [7],[8]. The frequency range of interest for conducted EMI in power electronics is usually from tens of kilohertz up to tens of megahertz [9]. Owing to the high switching speed of MOSFETs and IGBTs, the non-ideal behavior of the power converter plays an important role in the HF current component prediction. Thus, in order to model the HF behavior of the converter, it is necessary to take account of parasitic parameters in semiconductor devices and passive elements of the power circuit [10].

In the low and medium power range, the low voltage induction motor is the most frequently used type of motor. In this case, the winding is realized by a series connection of mush wound coils. Because of the random distribution of the turns in each coil, an analytical evaluation of the coil model parameters cannot be based on single-turn models such as in form wound coils [11]. Hence, the lumped equivalent circuit of a coil can be defined in terms of equivalent impedance by a suitable three-terminal circuit. Both the real and imaginary components of the impedance should be considered to properly model the coil behavior [12]. The model of a multi-coil stator winding can be derived from the single-coil model [13]. A three-phase induction motor can be regarded as a "black box" with one terminal for each motor phase and a terminal for the motor frame (ground). Thus, the equivalence is formulated in terms of phase-to-phase and phase-to-ground impedances. Both real and imaginary components are considered.

The system analyzed in this paper is shown in Fig. 1. Two Line Impedance Stabilization Networks (LISNs, 50Ω/50μH) are employed to decouple the DC source from the inverter. The proposed circuit model includes both the inverter and the induction motor. The HF current interferences at the input and output sides of the inverter are numerically evaluated by PSpice. In particular, common- and differential-mode current components are considered in order to emphasize the HF coupling between the DC link and the motor terminals. The time-domain analysis is carried out together with a frequency-domain analysis to determine the HF current harmonic spectrum. The calculated results are compared with the experimental tests obtained with a drive system prototype.

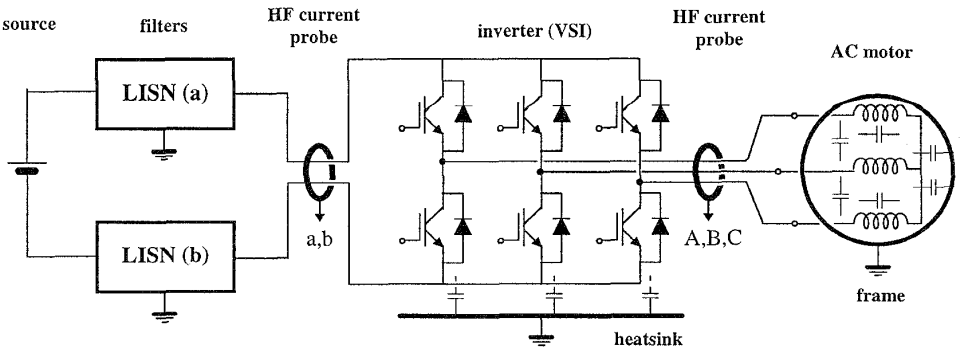

Fig. 1. Inverter-fed induction motor drive with DC LISN filters

0-7803-4489-8/98/$10.00 © 1998 IEEE

II. HF Circuit Models

In the system analyzed in this paper the length of the two cables connecting the LISNs to the inverter and the length of the three cables feeding the motor are about 1m. These power connections are simply modeled by series R-L circuits. More detailed circuit models for the inverter and the motor winding have been developed.

A. Inverter Model

In [10] an accurate circuit model for a switching cell, which is the basic structure of most power converters, has been presented and validated by experimental tests. In this paper the equivalent circuit of the three-phase Voltage Source Inverter (VSI) is obtained by an extension of the switching cell model. The ratings and the main characteristics of the inverter are given in Table I. Fig. 2 shows the HF equivalent circuit for one leg of the three-phase inverter including parasitic components. The converter analyzed in this paper is composed of three legs, each one consisting of two power IGBTs with parallel free-wheeling diodes. The models adopted for IGBTs and diodes are the PSpice general models. The models have been fitted with the parameter values given in the data sheets by using the "Parts" utility of PSpice. The effects of the IGBT and diode internal capacitances are included in the PSpice model, whereas the values of the collector and emitter internal inductances have been introduced in the inverter model on the basis of additional experimental data.

The HF circuit model of the system must take the main parasitic components of the inverter into account [14]. In particular, stray inductances of the capacitors and parasitic capacitances between the inverter and the ground are considered.

TABLE I
THREE-PHASE INVERTER RATINGS

	Type	Max. Voltage	Max. Current
IGBT (+diode):	3x SKM200GB122D	1200 V	150 A
Driver:	3x SKHI21		
Capacitors:	Electrolytic: 4x 1.5mF, Ceramic: 7x 0.33 μF		
Heatsink:	P16/300F - Forced air cooling		

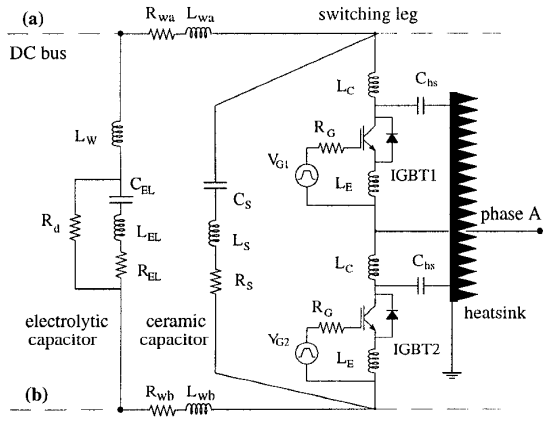

Fig. 2. HF circuit model for an inverter leg with parasitics

B. Motor Winding Model

Impedance measurements on different stator windings have demonstrated that the equivalent circuit represented in Fig. 3(a) can be adopted for both single-coil [12] and multi-coil AC windings [13],[14]. For three-phase windings, the mutual couplings among the phases should be introduced. In this paper the inductive coupling among the phases is taken into account by the mutual inductances M_1 and M_2 as represented in Fig. 3(b). The direct phase-to-phase capacitive coupling is neglected being the corresponding capacitances much lower than the phase-to-ground capacitances. The resulting circuit model, valid for three-phase AC windings, is represented in Fig. 3(b) [13].

In order to make the three-phase winding model fit with the experimental data, an identification problem must be solved. The model fitting can be performed either by a trial-and-error method or numerical techniques. A procedure to get an initial estimate of the model parameters is given in [13].

To verify the proposed model for three-phase motor windings, impedance measurements have been carried out at the induction motor terminals with the inverter disconnected. The motor data are given in Table II. The frequency behavior of both phase-to-phase and phase-to-ground impedances has been investigated. The measurements have been performed by a RLC meter HP 4192 with the frequency ranging from ten kHz to few MHz. The calculated and measured impedance values are shown in Figs. 4÷7. Figs. 4 and 5 are related to the phase-to-phase impedance. Fig. 6 and 7 illustrate the behavior of the phase-to-ground impedance. The solid lines represent the numerical results obtained with the circuit model, whereas the markers indicate the measured values.

TABLE II
THREE-PHASE INDUCTION MOTOR DATA

Power	Voltage, Frequency	Speed	Cooling
4 kW	220/380 V, 50 Hz	2800 rpm	coaxial fun

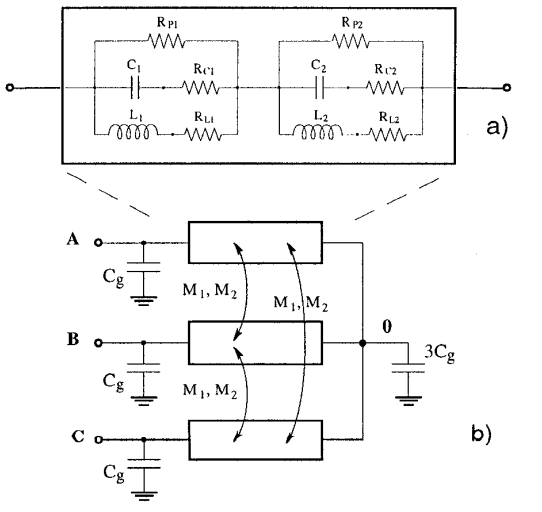

Fig. 3. Circuit model for a three-phase winding

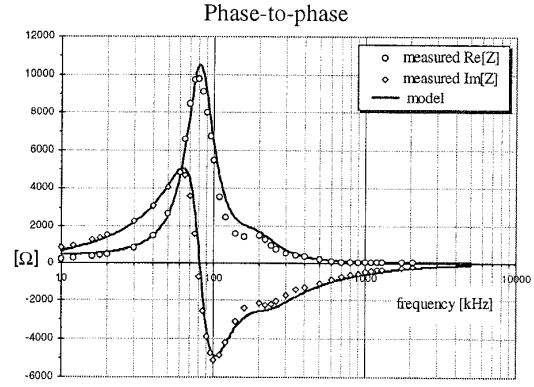

Fig. 4. Real and imaginary components of the impedance

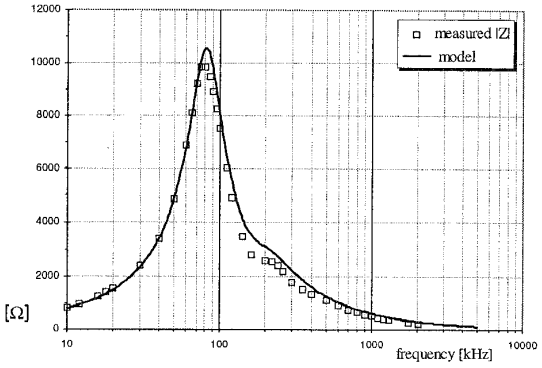

Fig. 5. Magnitude of the impedance

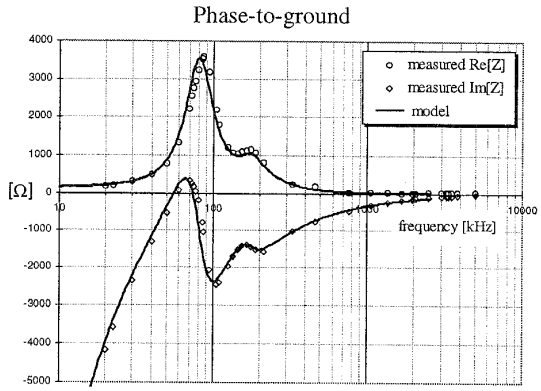

Fig. 6. Real and imaginary components of the impedance

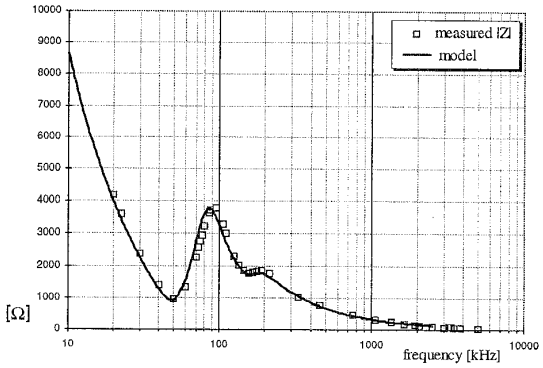

Fig. 7. Magnitude of the impedance

It can be noted that the agreement between numerical and experimental results is good in a wide frequency range even if all the circuit parameters have been assumed to be independent of the frequency. In order to improve the model matching for frequencies of few tens of kilohertz, frequency-dependent parameters should be adopted. In particular, a better fitting could be obtained by modeling skin and proximity effects with frequency-dependent resistances, and introducing frequency-dependent inductances to account for the magnetic reaction of eddy currents in the laminated core. By frequency-dependent parameters the circuit model could be usefully employed for frequency-domain analysis, whereas its application for time-domain analysis could be laborious. It has been verified that in most cases the improvements of the results obtained do not justify the increased model complexity.

III. CM and DM Current Detection

The conducted interferences have been analyzed both at the DC side, between the LISNs and the inverter, and at the AC side, between the inverter and the motor terminals.

For the two-wire system (DC side), the CM and DM current components are defined by the current signals i_a and i_b as follows

$$I_{CM} = \frac{1}{2}(i_a + i_b)\ ;\ I_{DM} = \frac{1}{2}(i_a - i_b)\,. \tag{1}$$

For the three-wire system (AC side), the CM current component is defined by the phase current signals i_A, i_B, and i_C as

$$I_{CM} = \frac{1}{3}(i_A + i_B + i_C)\,. \tag{2}$$

The DM current components can be defined for each phase as

$$I_{DM_k} = i_k - I_{CM}\ ,\ \text{for}\ k = A,\ B,\ C\,. \tag{3}$$

For phase A the previous equation yields

$$I_{DM_A} = I_{DM} = \frac{1}{3}(2i_A - i_B - i_C)\,. \tag{4}$$

Equation (4) is used to define the three-phase DM current component for balanced operating conditions.

The conducted interferences have been measured by HF current probes. When using magnetic probes with toroidal shape, a proper wire arrangement can be utilized to evaluate the CM and DM current components. Figs. 8 and 9 show the wire arrangements for 3-wire and 2-wire systems, respectively. In this way, a multiple of the CM and DM currents is directly evaluated avoiding an additional analog circuitry that could limit the bandwidth of the measuring system.

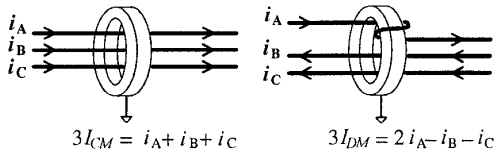

Fig. 8. Arrangement for the CM and DM current measurement for the 3-wire system (AC side)

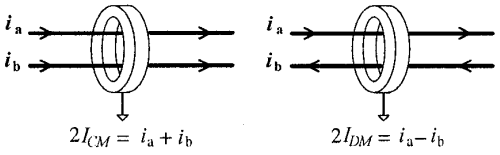

Fig. 9. Arrangement for the CM and DM current measurement for the 2-wire system (DC side)

IV. Numerical and Experimental Results

To validate the HF circuit model for the whole system, a prototype of inverter-fed AC motor drive has been realized. Measurements in both time- and frequency-domains have been carried out. The inverter has been controlled in the "six-steps mode" with a fundamental frequency of 10 kHz, that is the lower limit for the validity of the proposed HF circuit model. In this way, only current harmonics with frequency higher than 10 kHz flow in the system under investigation.

The LISNs (50Ω/50μH) have been introduced in order to decouple and standardize the inverter input from the DC source. The results presented in this paper have been obtained using a battery as DC source. The adopted measuring system was a Tektronix A6303 current probe (bandwidth from DC to 15 MHz) with the corresponding Tektronix AM 503B current probe amplifier. The measuring points are represented in Fig. 1 and the wire arrangements are shown in Figs. 8 and 9.

A. Time-Domain Analysis

The numerical analysis in the time domain has been performed by PSpice with an integration step ceiling of 50 ns. The corresponding experimental results have been recorded by a digital oscilloscope with a 50 Ω input adapter. The results are shown in Figs. 10 and 11, respectively. The agreement is good even if the dependence of all the model parameters on the excitation frequency has been neglected. This assumption allows numerical results to be achieved by a standard circuit simulator within reasonable computational times.

Figs. 10(a) and 11(a) represent the DM currents at the AC motor side. The current waveform is piecewise-linear and the frequency of its fundamental component is 10 kHz. The spikes are due to capacitive currents flowing through the phase-to-phase capacitive coupling owing to the high voltage time derivative (*dv/dt*) during the IGBTs commutations. It can be noted that the agreement is good for the amplitude of the fundamental component (1 A, 10 kHz), whereas the linear pieces have a little different slope. The explanation can be found in Sect. II.B with reference to Figs. 4 and 5: at 10 kHz the motor model has a good matching as regards the measured phase-to-phase impedance magnitude (Fig. 5), but the agreement is not so good for the real and imaginary components of the impedance (Fig. 4).

Figs. 10(b) and 11(b) represent the CM currents at the AC side. The waveform periodicity corresponds to a fundamental frequency of 30 kHz. Also in this case, the high *dv/dt* during the IGBTs commutations is responsible for the current spikes. The current oscillation following each spike has a frequency of about 100 kHz. This value corresponds to the resonant frequencies of

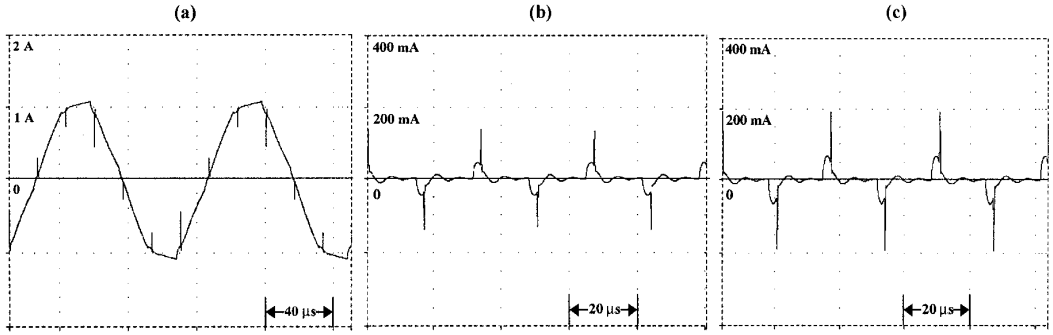

Fig. 10. Numerical results: (a) $3I_{DM}$ at AC side, (b) $3I_{CM}$ at AC side, (c) $2I_{CM}$ at DC side.

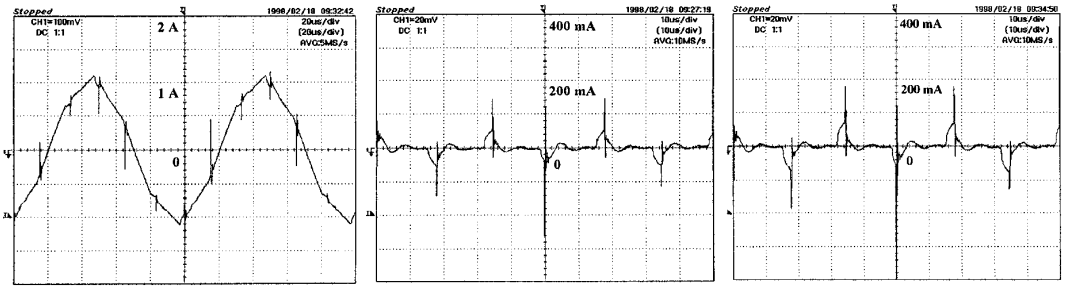

Fig. 11. Experimental results: (a) $3I_{DM}$ at AC side, (b) $3I_{CM}$ at AC side, (c) $2I_{CM}$ at DC side

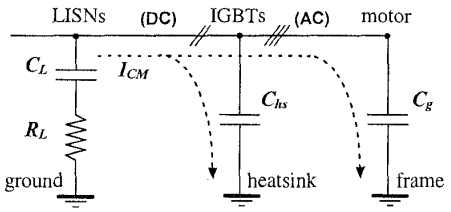

Fig. 12. Common-mode currents path.

the phase-to-ground impedance shown in Figs 6 and 7. The agreement between the numerical and the experimental results is very good.

Figs. 10(c) and 11(c) represent the CM currents at the DC side. It can be noted that these waveforms practically coincide with the CM current waveforms at the AC motor side except of a small scalar factor. The increase is caused by additional CM currents flowing through the IGBTs-to-heatsink parasitic capacitances, being the heatsink grounded for safety reasons. The CM current path is shown in Fig. 12. Also in this case the circuit model is able to predict the HF currents with a good accuracy.

The DM currents at the DC side have not been shown since their amplitudes are two order of magnitude less than those of the CM currents in the considered range of frequency. This is due to the filtering action performed by the DC capacitors (Table I, Fig. 2) that confine the DM currents inside the loops consisting of the switching legs and the capacitor branches.

B. Frequency-Domain Analysis

The numerical analysis in the frequency domain has been performed by post-processing the data obtained in the corresponding time-domain analysis. In this case, the Fourier facility of PSpice has been usefully employed. The experimental results have been obtained by a HP 8591E spectrum analyzer (bandwidth from 9kH to 1.8 GHz). The measurements were carried out selecting the peak mode. The frequency range was 10kHz÷2MHz and the results are shown in Figs. 13 and 14.

The fundamental frequency of the DM current components is 10 kHz. In particular, the numerical results represented in Fig. 13(a) show that the order of the harmonics is $6k\pm1$ with k an integer (i.e., 50-70 kHz, 110-130 kHz etc.). The agreement with the corresponding experimental results represented in Fig. 14(a) is good. It can be noted that the amplitude envelope of the DM current harmonics is very similar in the two cases, but additional harmonic components can be recognized in the experimental results.

The CM current components have a fundamental frequency of 30 kHz. Figs. 13(b) and 13(c) show that the order of the harmonics is $2k+1$ with k an integer (i.e., 90-150-210 kHz, etc.). The agreement with the corresponding experimental results represented in Figs. 14(b) and 14(c) is good. Also in this case, the calculated and measured amplitude envelopes of the CM current harmonics are very similar. Additional har-

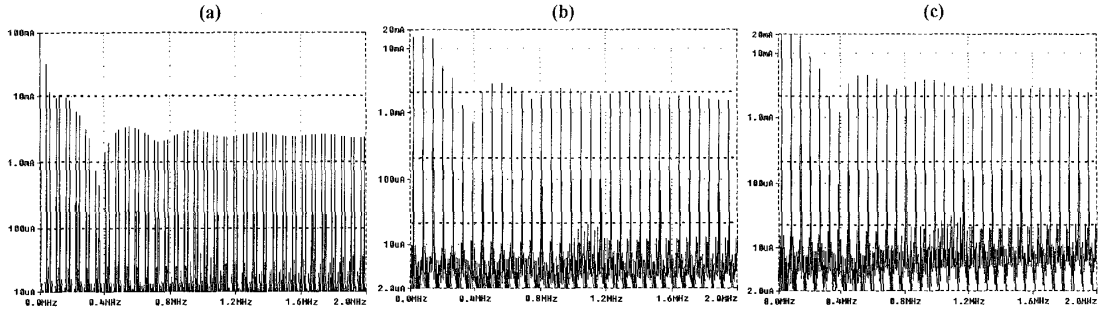

Fig. 13. Numerical results: (a) $3I_{DM}$ at AC side, (b) $3I_{CM}$ at AC side, (c) $2I_{CM}$ at DC side.

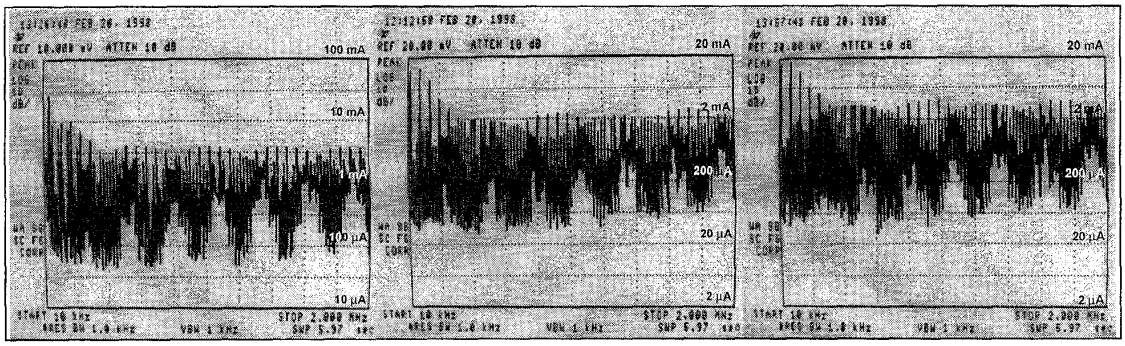

Fig. 14. Experimental results: (a) $3I_{DM}$ at AC side, (b) $3I_{CM}$ at AC side, (c) $2I_{CM}$ at DC side

monic components are present in the experimental results. It can be noted that the harmonic amplitudes are increased of about 3 dB at the DC side with respect to the AC side owing to capacitive currents through the grounded heatsink, as it could be expected analyzing Fig. 12.

IV. CONCLUSIONS

In this paper an inverter-fed AC motor drive is analyzed with reference to the conducted interferences at both the DC side and the AC motor side. Two LISNs are employed to decouple the DC source from the inverter. HF lumped equivalent circuits for the inverter and the motor stator winding are proposed. The inverter model includes parasitic components of power switches, passive components and connecting wires. The circuit model for the motor winding takes account of turn-to-turn and turn-to-ground stray capacitances. The model fitting is based on phase-to-phase and phase-to-ground impedance measurements. The overall system model has been tested with a system prototype in standard operating conditions with reference to the six-steps inverter mode. Using the equivalent circuit presented in this paper, the time-domain analysis can be performed with standard circuit simulators. The proposed model is particularly useful for the prediction of differential- and common-mode components of conducted EMI in a wide frequency range (10kHz÷2MHz). Guidelines for a overall system design satisfying the international EMC standards can be deduced. In particular, it has been shown that the CM current components strongly affect conducted interferences. The circuit model allows the effects of EMI suppression filters to be predicted by numerical simulations.

ACKNOWLEDGMENT

The Authors are grateful to Mr. Marco Matteini for his contribution to the set-up of the system prototype and for his help in the experimental tests.

REFERENCES

[1] L. Gubbala, A. von Jouanne, P. Enjeti, C. Singh, H. Toliyat, "Voltage Distribution in the Windings of an AC Motor Subjected to High dv/dt PWM Voltages," *Proc. of PESC Conference*, June 1995, Atlanta (USA), pp. 579-585.

[2] Z. Krzemien, "The Additional Phenomena which Appear in Induction Motors Fed from PWM Inverters," *European Conf. on Power Electronics & Applications, EPE*, September 1997 - Trondheim (N), pp. 2.515-2.519.

[3] D.Maly, D.W.Novotny, C.Thompson, "The Influence of Winding Capacitance on High Frequency Time Harmonic Losses in Induction Motors," 0-7803-0634-1/92, *IEEE*, pp. 33-39.

[4] Y. Murai, T Kubota, Y Kawase, "Leakage Current Reduction for a High-Frequency Carrier Inverter Feeding an Induction Motor," *IEEE Trans. on Ind. Appl.*, Vol. 28, No. 4, July/Aug 1992, pp. 858-863.

[5] E. Zhong, S. Chen, T.A. Lipo, "Improvements in EMI Performance of Inverter-Fed Motor Drives," *Proc. of APEC*, March 1994, pp. 608-614.

[6] E. Zhong, T.A. Lipo, J.R. Jaeschke, D. Gritter, "Analytical Estimation and Reduction of Conducted EMI Emission in High Power PWM Inverter Drives," *Proc. of PESC Conference*, June 1996, Baveno (IT), pp. 1169-1175.

[7] A. Consoli, G. Oriti, A. Testa, "Induction Motor Modelling for Common Mode and Differential Mode Emission Evaluation," *IEEE IAS Conf.*, October 1996, S.Diego (USA), pp. 595-599.

[8] S. Ogasawara, H. Hirofumi, "Modelling and Damping of High-Frequency Leakage Currents in PWM Inverter-Fed AC Motor Drive Systems," *IEEE Trans. on Industry Applications*, Vol. 32, No. 5, September/October 1996, pp. 1105-1114.

[9] L. Tihanyi, *Electromagnetic compatibility in power electronics*. IEEE Press 1995, New York (USA).

[10] G. Grandi, I. Montanari, U. Reggiani, "Effects of power converter parasitic components on conducted EMI," *International Zurich Symposium on EMC*, 18-20 February 1996, Zurich (CH), pp. 499-504.

[11] R.G. Rhudy, E.L. Owen, D.K. Sharma, "Voltage Distribution Among the Coils and Turns of a Form Wound AC Rotating Machine Exposed to Impulse Voltage," *IEEE Trans.*, Vol. EC-1, No. 2, June 1986, pp. 50-60.

[12] G. Grandi, D. Casadei, U. Reggiani, "Equivalent Circuit of Mush Wound AC Windings for High Frequency Analysis," *Proc. ISIE Conf.*, July 1997, Guimarães (PT), pp. SS.201-SS.206.

[13] G. Grandi, D. Casadei, A. Massarini, "High Frequency Lumped Parameter Model for AC Motor Windings," *European Conf. on Power Electronics & Applications, EPE*, September 1997 - Trondheim (N), pp. 2.578-2.583.

[14] S. Guttowski, H. Jorgensen, K. Heumann, "The Possibilities of Reducing Conducted Line Emissions by Modifying the Basic Parameters of Voltage-Fed Pulsed Inverters," *IEEE PESC'97*, June 1997, St. Louis, Missouri, pp. 1535-1540.

[15] J.L. Guardado, K.J. Cornik, "Calculation of Machine Winding Electrical Parameters at High Frequencies for Switching Transient Studies," *IEEE Trans. on Energy Conversion*, Vol. 11, No. 1, March 1996, pp. 33-40.